An Optimization-Based Initial Position Estimation Method for Switched Reluctance Machines

Lefei Ge, *Member, IEEE*, Huihui Xu, *Student Member, IEEE*, Zhenchao Guo, Shoujun Song, *Senior Member, IEEE*, and Rik W. De Doncker, *Fellow, IEEE*

***Abstract*—A new method to detect the initial rotor position of switched reluctance machine (SRM) is presented in this article. Unlike most conventional position estimation methods, the proposed method does not need any extra premeasurement and only the data with finite element method (FEM) are required. First, a linear regression model (LRM) is presented to describe the relationship between FEM and measured inductance characteristics. Then, to detect the position, the residual sum of squares of the proposed LRM is considered as an objective function, which is a convex function with rotor position. The rotor position can be estimated by minimizing the objective function with the golden-section search method. Finally, the accuracy of the proposed estimation algorithm is validated by the experimental results on a three-phase 12/8 pole SRM prototype. Compared with the existing position estimation methods, the proposed method has higher accuracy and less measurement effort. The proposed method can serve as a supplement to provide accurate initial position information for incremental position sensors.**

***Index Terms*—Golden-section search (GSS) method, initial position estimation, linear regression model (LRM), switched reluctance machine (SRM).**

I. Introduction

SWITCHED reluctance machines (SRMs) have received increasing attention for various kinds of industrial applications due to their low cost and rugged structure [1]–[3]. However, their operations, especially for high-performance control, need accurate rotor position information. The mechanical rotor position sensors are usually required to provide position information. The sensors for position detection of SRMs can be classified into absolute position sensors and incremental position sensors. Absolute sensors, such as the resolver, can provide unique position information for each shaft angular location, including the initial rotor position [4]. However, the cost of these sensors is much higher than that of the incremental ones. For the low-end drive application, the incremental position sensors, such as optical sensors and Hall sensors, are more widely used [5].

To obtain the initial rotor position for incremental position sensors, the rotor is rotated to the aligned position first by applying a high-level current pulse to the specific phase windings [6]. The force-aligned method is simple and easy to be implemented. However, the accuracy of rotor position detection cannot be ensured if the load is already connected to the rotor shaft. Besides, the start-up time is increased because of mechanical alignment, which is especially serious for the application with high inertia load, such as electric vehicles. Therefore, it is essential to find an accurate initial rotor position estimation to extend the application of incremental position sensors.

Various sensorless methods for rotor position estimation have been widely reported in recent years. Most sensorless publications, such as state-observer-based methods [7], [8], phase-locked loop based methods [9], [10], filter-based methods [11], [12], and special position detection based methods [13], [14], are focused on the medium and high speed range. Threshold-based methods [15], core-loss-based method [16], and current-gradient-based methods [17] can be used to estimate the rotor position in the low-speed range. However, it is still a challenge to achieve an accurate initial position estimation at a standstill. The initial rotor position estimation methods can be divided into two categories depending on whether or not the premeasured data are required. The main challenge in obtaining the initial rotor position is to balance the cost of the premeasurement and the accuracy of the rotor position estimation. In [18], all the phase windings are excited for a short moment, and the initial position is estimated based on a prestored flux-linkage table from the phase with the maximum current. In [19], the time required for reaching a threshold current is recorded and the initial rotor position is computed from the phase with a linear relationship between the rotor position and the measured time. Bu and Xu [18] and Krishnamurthy *et al.* [19] can get an accurate initial rotor position information, but the measurement of the flux-linkage table or the required time is very complex and time-consuming. In [20], the unsaturated inductance profile is measured by recording the current waveform when the SRM is driven by a prime motor at a constant speed, and the initial rotor position can be calculated by the premeasured inductance profile. The measurement of automation and intelligence is improved in this method, but it is only suitable for the test bench with a prime motor. In [21], a bootstrap-circuit-based

Manuscript received November 19, 2020; revised March 19, 2021; accepted May 13, 2021. Date of publication May 18, 2021; date of current version July 30, 2021. This work was supported in part by the National Natural Science Foundation of China (51877179) and in part by the Fundamental Research Funds for the Central Universities (3102021ZDHQD03). Recommended for publication by Associate Editor E. Armando. *(Corresponding author: Lefei Ge.)*

Lefei Ge, Zhenchao Guo, and Shoujun Song are with the Northwestern Polytechnical University, Xi'an 710072, China (e-mail: lge@nwpu.edu.cn; 15991262370@163.com; sunnyway@nwpu.edu.cn).

Huihui Xu and Rik W. De Doncker are with the Institute for Power Electronics and Electrical Drives, RWTH Aachen University, 52062 Aachen, Germany (e-mail: Huihui.Xu@isea.rwth-aachen.de; dedoncker@ieee.org).

Color versions of one or more figures in this article are available at https://doi.org/10.1109/TPEL.2021.3081618.

Digital Object Identifier 10.1109/TPEL.2021.3081618

method is proposed and the initial rotor position is estimated based on the time required for reaching the maximum charging current of the bootstrap circuit. This method eliminates the EMI influence caused by the injection narrow width pulses, but the extra hardware circuit raises its implementation complexity. Although the sensorless methods with premeasured data can get satisfactory position estimation results, they have the following disadvantages that should be considered.

1) Extra test bench is usually required to perform the characteristic measurement of flux-linkage, time, peak current, or inductance. It is very costly and time-consuming for the design and test of the extra test bench.
2) The high-precision absolute position sensors are usually indispensable to record the characteristic data, which increase the complexity and cost.
3) The test bench has to be adjusted or even redesigned as the ratings and overall dimensions of SRMs [22].

Therefore, it is necessary to find a sensorless method without any extra premeasurement. General inductance model based methods (GIMMs) are proposed in [23] and [24]. In [23], a quadratic polynomial regression model is used to describe the relative inductance, and the rotor position is estimated by curve fitting. A similar method is found in [24] except that the type-V exponential regression is used instead of the polynomial regression model, and higher accuracy is achieved. These methods do not require any extra premeasurement, but the accuracy of the rotor position heavily relies on the fitness between the actual and assumed model. Coordinate-transformation-based methods (CTMs) [25], [26] are another effective way to estimate the initial rotor position. The main idea of these methods is that the phase inductance profile can be fitted by the first-order Fourier series neglecting the high-order components, and the inductance in the three-phase coordinate system can be transformed into the two-phase $\alpha - \beta$ coordinate system by using Clark coordinate transformation. Then, the initial rotor position can be estimated with transformed inductance in a two-phase $\alpha - \beta$ coordinate system. Traditionally, this method is only suitable for the three-phase machine. Gan *et al.* [27] propose a method to extend its application for multiphase SRMs. However, the accuracy of the rotor position is limited for neglecting the high-order components. This article proposes an optimization-based method to estimate the initial rotor position based on the linear regression model (LRM) between simulated and measured inductance. Compared with the existing literature research efforts, the proposed method has the following features.

1) Compared with traditional sensorless methods with premeasured data, the proposed method does not require any extra premeasurement, which effectively reduces the cost and measurement effort.
2) Compared with other sensorless methods without premeasured data, such as GIIMs and CTMs, the proposed methods have higher accuracy for the rotor position estimation.

This article is organized as follows. Section I starts with the literature review about the position estimation methods and clarifies the novelty of the proposed method. The methods to calculate the unsaturated phase inductance characteristic by measurement and finite element method (FEM) simulation are introduced in Section II. In Section III, an LRM is presented to describe the relationship between FEM and measured inductance characteristics. The rotor position can be estimated by minimizing the residual sum of squares (RSS) of the proposed LRM with the golden-section search (GSS) method. Section IV verifies the accuracy of the proposed estimation algorithm on a three-phase 12/8-pole SRM prototype. The influence of the accuracy of the measured inductance on the rotor position estimation is discussed in Section V. Finally, Section VI concludes this article.

II. Unsaturated Phase Inductance Characteristic

The estimation of the initial rotor position depends on the unsaturated phase inductance characteristic of SRMs. It can be obtained by measurement or FEM simulation.

A. Measurement

To estimate the phase inductance with measurement, a high-frequency pulse signal should be injected into one phase at a certain position. The phase current slope difference method in [26] is introduced in this section to estimate the phase inductance. At a standstill, the back electromotive force can be omitted as there is no rotor movement. Besides, the saturation effect can be also neglected with a low-current peak value. Thus, the voltage balance equation can be simplified as

$$V_{\rm ph} = R_{\rm ph} i_{\rm ph} + L_{\rm ph} \frac{di_{\rm ph}}{dt} \tag{1}$$

where $V_{\rm ph}$, $R_{\rm ph}$, $i_{\rm ph}$, and $L_{\rm ph}$ represent phase voltage, phase resistance, phase current, and phase inductance, respectively.

When the converter works in the turn-ON mode, the phase voltage can be deduced from the bus voltage by excluding the power switches drop $V_{\rm T}$, which is given as

$$V_{\rm ph} = R_{\rm ph} i_{\rm ph} + L_{\rm ph} \frac{di_{\rm ph}}{dt}|_{\rm on} = V_{\rm dc} - 2V_{\rm T}. \tag{2}$$

When the converter works in the turn-OFF mode, the phase voltage $V_{\rm ph}$ can be expressed as

$$V_{\rm ph} = R_{\rm ph} i_{\rm ph} + L_{\rm ph} \frac{di_{\rm ph}}{dt}|_{\rm off} = -V_{\rm dc} - 2V_{\rm D} \tag{3}$$

where $V_{\rm D}$ is the diode voltage drop.

By subtracting (2) and (3), the unsaturated phase inductance can be obtained, which is expressed as

$$L_{\rm ph} = \frac{2V_{\rm dc} + 2(V_{\rm D} - V_{\rm T})}{\frac{di_{\rm ph}}{dt}|_{\rm on} - \frac{di_{\rm ph}}{dt}|_{\rm off}}. \tag{4}$$

The current slope is assumed as constant in the rising and falling stages, as shown in Fig. 1. The online linear least-square fit (OLSF) is adopted to estimate the current slope

$$\frac{di_{\rm ph}}{dt} = \frac{\sum_{k=1}^{N} \left(t(k) - \frac{1}{N}\sum_{k=1}^{N} t(k)\right)\left(i_{\rm ph}(k) - \frac{1}{N}\sum_{k=1}^{N} i_{\rm ph}(k)\right)}{\sum_{k=1}^{N} \left(t(k) - \frac{1}{N}\sum_{k=1}^{N} t(k)\right)^2} \tag{5}$$

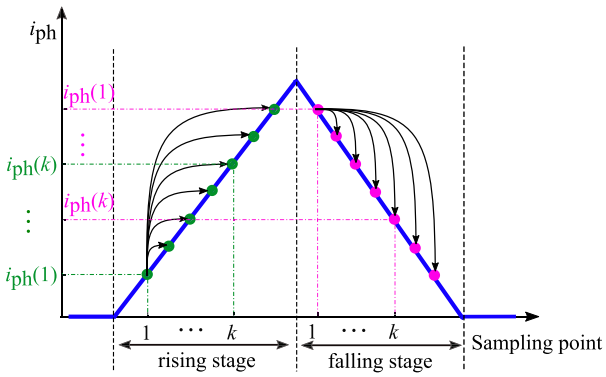

Fig. 1. Phase current slope calculation after pulse signal injection.

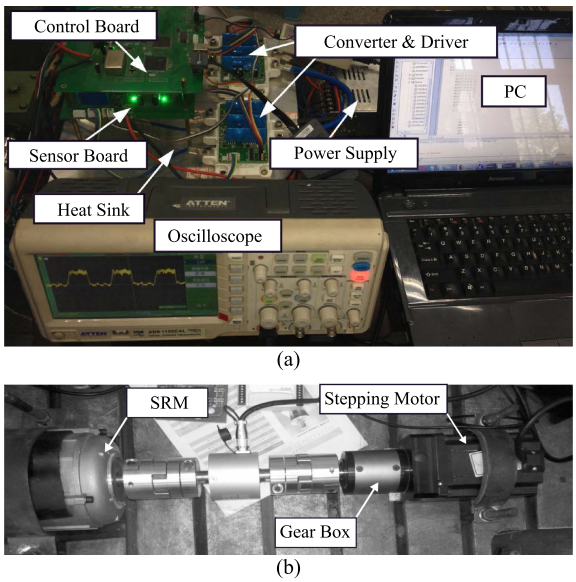

Fig. 2. Test bench. (a) Electrical part. (b) Mechanical part.

where $t(k)$ and $i_{\text{ph}}(k)$ are the sampled time and the sampled phase current, respectively. N is the number of sampling points in the rising or falling stages. A SRM with 3-phase 12/8 pole configuration is considered as an exemplary prototype in this paper. The ratings and parameters of the SRM prototype are provided in Appendix. Fig. 2 shows the photograph of the experimental test bench.

B. Finite Element Method

Due to the development of computer technology, FEM is becoming more and more popular in the performance analysis of electrical machines. It has proved to be a convenient and accurate method by many researchers. However, its accuracy depends on the exact geometrical dimensions, material properties, and winding placement [3]. These parameters provided by the manufacturers are not always accurate and the electromagnetic properties of the ferromagnetic material may change during the manufacturing process [28]. In [29], it claims that the actual air gap could be different than that shown on the datasheet because

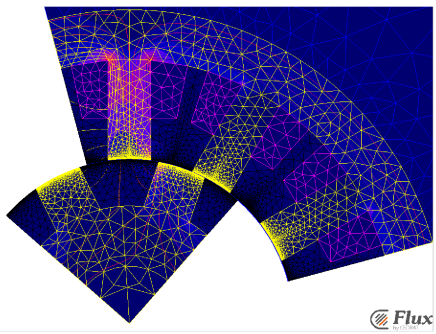

Fig. 3. FEM model of the experimental SRM in Flux2D.

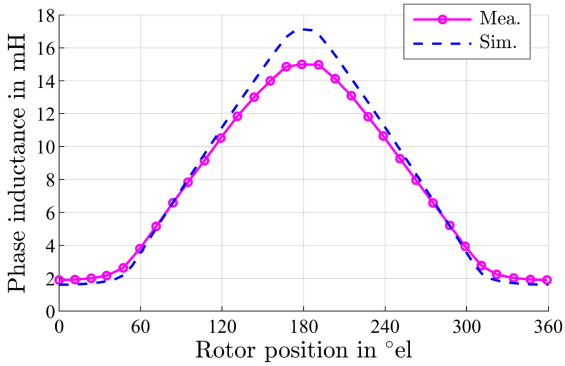

Fig. 4. Comparison of unsaturated phase inductance between the measurement and FEM simulation results.

of the complication of the manufacturing process, which yields a significant difference between the measured and simulated results. Compared with measurement, FEM is a less accurate but low-effort way to obtain the unsaturated phase inductance characteristic. The FEM model of the exemplary machine is built in the commercial FEM software Flux2D, which is shown in Fig. 3. Due to the symmetry of SRM configuration, only one-fourth of the machine requires to be considered for the simulation. By applying low-level current to one phase winding for all positions, the unsaturated phase inductance characteristic can be simulated.

The measured unsaturated inductance characteristics are compared with the FEM results, as shown in Fig. 4. In Fig. 4, the symbol of "el" represents for electrical degree. The measured inductance values are marked by the circle and connected into the line forming the measured inductance profile. It can be observed that relatively large errors happen at the aligned position. It might be caused by the wrong airgap parameters caused by the manufacturing process. Although these two curves are not coincided, the inductance curve by FEM simulation is similar to that obtained by measurement, which indicates a linear relationship between measurement and FEM simulation results.

III. Proposed Position Estimation Method

A. Linear Regression Model

To evaluate the correlation between these two parameters, the Pearson product-moment correlation coefficient is introduced,

which is defined as

$$r = \frac{\sum_{i=1}^{n}(L_{\text{sim},i} - \bar{L}_{\text{sim}})(L_{\text{mea},i} - \bar{L}_{\text{mea}})}{\sqrt{\sum_{i=1}^{n}(L_{\text{sim},i} - \bar{L}_{\text{sim}})^2}\sqrt{\sum_{i=1}^{n}(\bar{L}_{\text{mea},i} - \bar{L}_{\text{mea}})^2}} \tag{6}$$

where n is the sample size, L_{sim} and L_{mea} are the sample points of simulated and measured inductance, respectively, and $\bar{L}_{\text{sim}}$ and $\bar{L}_{\text{mea}}$ are their mean values. The calculated r for the employed SRM is 0.9993, which depicts a very good linear relationship. Hence, an LRM can be adopted to find the linear expression between the simulated and measured inductance, which is expressed as

$$L_{\text{mea}} = \alpha + \beta L_{\text{sim}} + \epsilon \tag{7}$$

where α and β are coefficients. ϵ is the estimation error.

The least-square method is adopted to estimate the coefficients. Its core idea is to minimize the RSS, which is expressed as

$$Q(\alpha, \beta) = \min \text{RSS}(\alpha, \beta) = \min \sum_{i=1}^{n}(L_{\text{mea},i} - \alpha - \beta L_{\text{sim},i})^2. \tag{8}$$

The minimum of $\text{RSS}(\alpha, \beta)$ is found by setting the gradient to zero. Therefore, the gradient equations can be given by

$$\begin{cases} \frac{\partial Q}{\partial \alpha} = -2\sum_{i=1}^{n}(L_{\text{mea},i} - \hat{\alpha} - \hat{\beta} L_{\text{sim},i}) = 0 \\ \frac{\partial Q}{\partial \beta} = -2\sum_{i=1}^{n} L_{\text{sim},i}(L_{\text{mea},i} - \hat{\alpha} - \hat{\beta} L_{\text{sim},i}) = 0 \end{cases} \tag{9}$$

where $\hat{\alpha}$ and $\hat{\beta}$ are the estimated values of α and β, respectively. Then, $\hat{\alpha}$ and $\hat{\beta}$ can be derived by

$$\begin{cases} \hat{\alpha} = \bar{L}_{\text{mea}} - \hat{\beta}\bar{L}_{\text{sim}} \\ \hat{\beta} = \frac{\sum_{i=1}^{n} L_{\text{sim},i} L_{\text{mea},i} - n\bar{L}_{\text{sim}}\bar{L}_{\text{mea}}}{\sum_{i=1}^{n} L_{\text{sim},i}^2 - n\bar{L}_{\text{sim}}^2}. \end{cases} \tag{10}$$

B. Optimization-Based Position Estimation Method

For the machine with phase number N_{ph}, the measured inductance dataset $L_{\text{mea},i}$ (i=1,2,. . ., N_{ph}) with real-time computation from the phase current and voltage can be simultaneously estimated with pulse signal injection method [30]. However, the simulated inductance dataset $L_{\text{sim},i}$ (i=1,2,. . ., N_{ph}) is unknown, because the rotor position is not available. To estimate the rotor position, an objective function based on the RSS of the LSM is presented, which is defined as

$$\text{RSS}(\theta) = \sum_{i=1}^{N_{\text{ph}}}(L_{\text{mea},i} - \hat{\alpha} - \hat{\beta} L_{\text{sim},i}(\theta))^2. \tag{11}$$

As stated in the previous section, the measured and simulated data have an approximately linear relationship. Therefore, the objective function will find its minimum at the actual position, theoretically. In this way, the rotor position estimation is converted to the function optimization problem. Before optimization, the interval and initial value of θ should be specified. The interval of θ can be determined by comparing the amplitudes of the measured phase inductance. As an example, the inductance profile for the three-phase machine is shown in Fig. 5. From this figure, we can observe that there is a one-to-one mapping between the order of the measured phase inductance and the interval of θ. The rules of θ interval determination for the three-phase machine are listed in Table I.

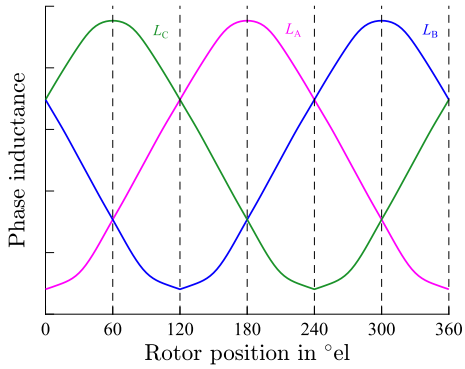

Fig. 5. Inductance profile for the three-phase machine.

TABLE I
RULES OF INTERVAL DETERMINATION FOR THE THREE-PHASE MACHINE

Rules	$L_A \le L_B < L_C$	$L_B \le L_A < L_C$	$L_B \le L_C < L_A$
Interval	[0 °el, 60 °el)	[60 °el, 120 °el)	[120 °el, 180 °el)
Rules	$L_C \le L_B < L_A$	$L_C \le L_A < L_B$	$L_A \le L_C < L_B$
Interval	[180 °el, 240 °el)	[240 °el, 300 °el)	[300 °el, 360 °el)

The GSS method is adopted to find the minimum of the objective function. Its basic idea is to narrow the search interval containing the minimum value by comparing the function values of trial points until the interval is narrowed down to a given accuracy [31]. The detailed process of the application of GSS to position estimation is concluded as follows.

1) Determine the initial interval of rotor position [a, b] by comparing the measured phase inductance with Table I. Set the convergence accuracy ϵ, such as 0.1° el.
2) Compute the trial points p and q based on (12) and evaluate the objective functions $\text{RSS}(p)$ and $\text{RSS}(q)$ at trail points with the method proposed in previous section

$$\begin{cases} p = b - r(b - a) \\ q = a + r(b - a) \end{cases} \tag{12}$$

   where r is the golden ratio and its approximate value is 0.618.
3) Update the interval by comparing $\text{RSS}(p)$ and $\text{RSS}(q)$. If $\text{RSS}(p) < \text{RSS}(q)$, set $a = a$ and $b = q$; else, set $a = p$ and $b = b$.
4) Check if the terminal condition $|a - b| \le \epsilon$ has been achieved. If yes, continue to the next step; else, repeat steps (2) to (4).
5) Take the mean value of a and b as the estimated rotor position $\hat{\theta}$.

To give the readers a better understanding of the proposed method, a flowchart is presented in Fig. 6. The pulse voltage

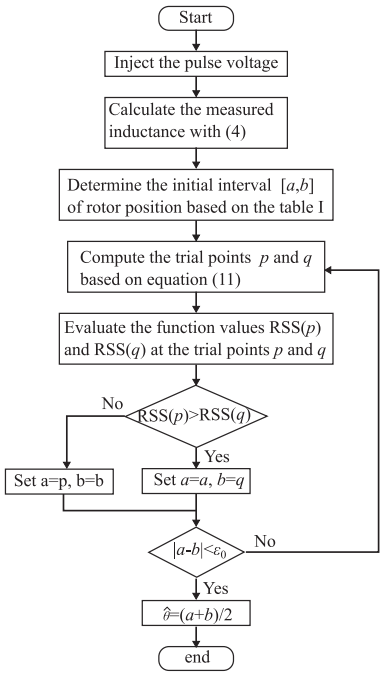

Fig. 6. Flowchart of the proposed initial position estimation method.

injection is the same as the traditional rotor position estimation methods [30]. However, the rotor position estimation accuracy can be improved by making full use of the prior machine data, which will be verified in detail in the next section.

IV. Experimental Verification

To verify the accuracy and effectiveness of the proposed position estimation method, experiments are carried out on the three-phase 12/8 pole SRM prototype in this section.

To verify the accuracy of the proposed method at each position in one electrical period, the three-phase current data are obtained for each 12° el by injecting PWM voltage pulse. The bus voltage is 20 V, and the frequency and duty cycle of the voltage pulse are 1 kHz and 0.4, respectively. As an example, the measured current waveforms and voltage waveform at 35° el are presented in Fig. 7. Fig. 8 shows the position estimation process at this position. It can be seen that $\mathrm{RSS}(\theta)$ is a convex function at the interval $[a, b]$ with minimum at actual position. In Fig. 7, the order of the phase current is $i_{\mathrm{C}} \leq i_{\mathrm{B}} < i_{\mathrm{A}}$. Thus, the order of the phase inductance is $L_{\mathrm{A}} \leq L_{\mathrm{B}} < L_{\mathrm{C}}$. From Table I, the initial values of a and b are 0 and 60, respectively. Then, p and q are calculated with (12). By repeating the search process, the values of a, b, p, and q are constantly updated till the difference between a and b is smaller than the convergence accuracy ϵ. After 15 iterations with GSS, the absolute value of the difference interval parameters a and b converges within 0.1° el. Then, the rotor position can be estimated by their mean value, which is 33.69° el.

The rotor position estimation results and errors for the whole electrical period with proposed method are presented in Figs. 9 and 10. The stepping machine introduced in Section II is employed to ensure that the whole electrical period is evaluated. For comparison, the estimation results with CTM in [26] and GIMM in [24] are also presented Figs. 9 and 10 . The results show that the proposed method has better accuracy for position estimation.

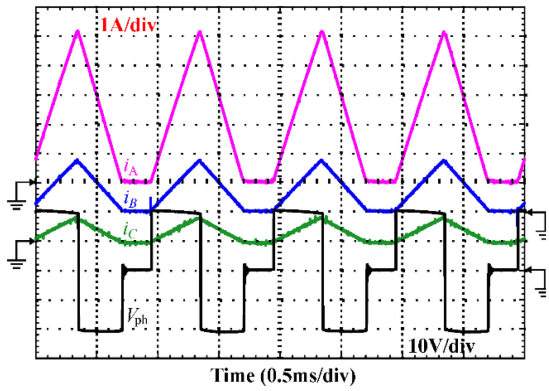

Fig. 7. Measured current waveforms for all phases and injected voltage waveform at 35° el.

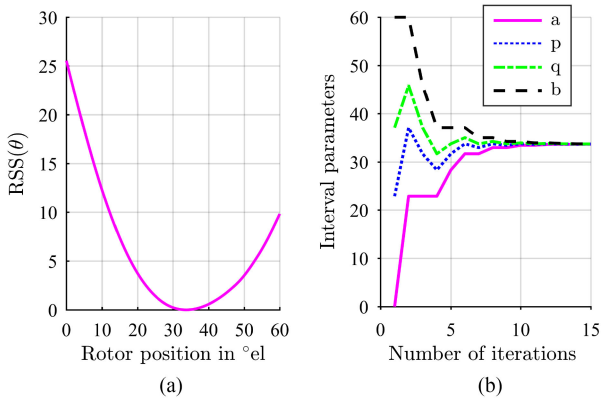

Fig. 8. Rotor position estimation at 35° el. (a) Objective function. (b) Optimization process.

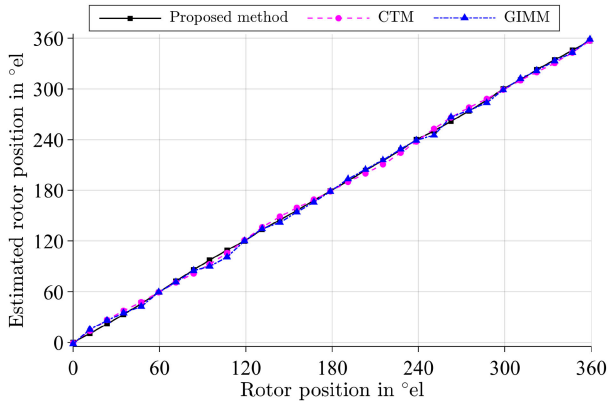

Fig. 9. Rotor position estimation for one electrical period.

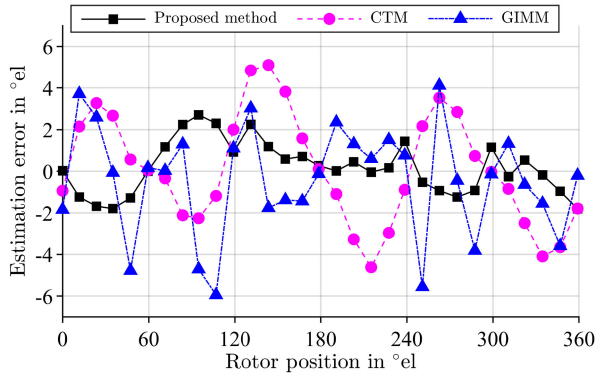

Fig. 10. Estimation error of rotor position for one electrical period.

TABLE II
ERROR COMPARISON WITH DIFFERENT METHODS

Methods	Proposed method	CTM	GIMM
MAVE	2.19 °el	5.10 °el	5.94 °el
RMSE	0.98 °el	2.63 °el	2.63 °el

To quantitatively evaluate the accuracy of each method, two types of errors are introduced, which are the maximum absolute value of error (MAVE) and root-mean-square error (RMSE), respectively. Their definitions are given in (13) and (14). Table II lists the comparison of different methods for MAVE and RMSE. It can be seen that the MAVE of the proposed method is only 2.19° el (0.27° for mechanical angle), which is at least two times smaller than CTM and GIMM. Furthermore, the RMSE of the proposed method is 0.98° el, which is at least 2.5 times smaller than CTM and GIMM. Based on the aforementioned results, it is obvious that the proposed method offers the most accurate estimation of the rotor position. In the proposed method, the FEM simulation data are employed to construct the objective function. Compared with the model in CTM and GIMM, the FEM simulation data contain the high-order components of the inductance model and have better fitness than an assumed mathematic model. Therefore, the estimation results with the proposed method can achieve the highest accuracy

$$\mathrm{MAVE} = \max_{j=1}^{m} |e_j| \tag{13}$$

$$\mathrm{RMSE} = \sqrt{\frac{1}{n}\sum_{j=1}^{n} e_j^2} \tag{14}$$

where e is the error of rotor position estimation.

Fig. 11 compares the computation time in DSP for the proposed method, CTM, and GIMM. It can be seen that the computation time of CTM is the shortest because of its simplicity. The GIMM is the most time-consuming because of the complex mathematical operations. It takes 156.8 μs for the proposed method to finish the search process, which is faster than GIMM but much slower than CTM. It should be noted that the computation time is less important compared with the accuracy since the purpose of this article is to determine the initial rotor position for incremental position sensors.

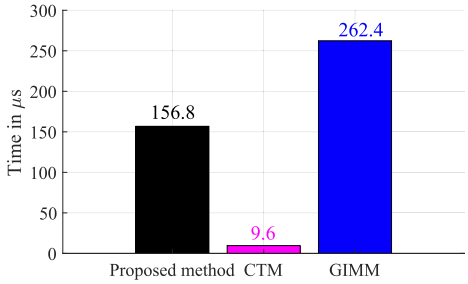

Fig. 11. Computation time comparison for the proposed method, CTM, and GIMM.

TABLE III
ERROR COMPARISON WITH SCALING ERRORS

Methods	original	one phase	two phase	three phase
MAVE	2.19 °el	2.49 °el	2.45 °el	2.71 °el
RMSE	0.98 °el	1.09 °el	1.1 °el	1.25 °el

V. DISCUSSION

The proposed method can effectively improve the accuracy of the rotor position estimation. However, the proposed method still relies on measured inductance. Therefore, the effect of the accuracy of the measured inductance on the proposed method should be discussed.

The errors of measured inductance come from both the calculation errors and sensor errors. The differential form is adopted to calculate the phase inductance, which will introduce calculation errors to the results. To reduce the calculation errors, the least square method in [3] is introduced to minimize the RSS. Besides, the selection of sampling frequency is crucial for calculation errors. A low sampling frequency will increase the truncation error of numerical calculation. But too high frequency will raise the computation burden and the rounding errors. In this article, the adopted sampling frequency in DSP is 20 kHz.

The current sensor errors are another source of errors of measured inductance. The measurement errors of current sensors can be divided into offset errors and scaling errors [32]. The differential form in (4) indicates that the scaling errors of current sensors should be the main source of the error of measured inductance. The measured currents are detected by Hall effect current sensors LA55-P. From its datasheet [33], we can conclude that the maximum of scaling errors is 0.65%. The scaling errors may exist in one phase or multiphase. The influence of the scaling errors of current sensors on the MAVE and RMSE of the rotor position estimation are presented in Table III. From this table, it can be seen that the accuracy of the rotor position estimation varies with the scaling errors of the current sensors. However, the variation of accuracy is in the range of allowable error.

In Section II, the phase current slope is assumed to be time invariant to calculate the phase inductance. However, the phase

TABLE IV
ERROR COMPARISON WITH DIFFERENT TYPES OF CURRENT SLOPE

Methods	OLSF	Maximum	Minimum
MAVE	2.19 °el	2.43 °el	3.45 °el
RMSE	0.98 °el	1.25 °el	1.23 °el

current slope is time varying as we can conclude from (15) due to the variation of the phase current. Therefore, the influence of the approximation of the current slope on position estimation should be discussed

$$\frac{di_{\text{ph}}}{dt} = \frac{V_{\text{ph}} \text{-} R_{\text{ph}} i_{\text{ph}}}{L_{\text{ph}}}. \tag{15}$$

From (15), it can be concluded that the maximum and minimum values of the current slope are located at the moments when the phase current is zero and its peak value, respectively. Table IV presents the position estimation errors with the OLSF, maximum, and minimum values of the current slope. From Table IV, we can conclude that the time-varying current slope introduces additional errors for the position estimation. Besides, it is a reasonable choice to use the OLSF to reduce the errors caused by the time-varying current slope.

VI. CONCLUSION

An optimization-based position estimation method for SRMs is proposed in this article. In this method, an objective function is built based on the RSS of measured and simulated inductance. A GSS method is employed to find its minimum, which locates at the actual position due to the linear relationship between measured and simulated data. The experimental results show the proposed method has high accuracy at all positions. The proposed method is simple and only contains elementary arithmetic, which is very easy to be implemented in the microprocessor. Furthermore, it does not need any extra premeasurement and the accuracy is less than 0.27° for the investigated machine.

APPENDIX

The geometric parameters of the SRM prototype are listed in Table V.

TABLE V
GEOMETRIC PARAMETERS OF THE PROTOTYPE

Parameter	Value	Parameter	Value
Number of phase	3	Stator yoke thickness	9.5 mm
Number of stator pole	12	Rotor yoke thickness	11.5 mm
Number of rotor pole	8	Number of turns	119
Rated power	1 kW	Stack length	81 mm
Rated speed	2000 rpm	Airgap length	0.15 mm
Stator radius	60 mm	Stator pole arc	15°
Rotor radius	31.35 mm	Rotor pole arc	17°

REFERENCES

[1] H. Li, B. Bilgin, and A. Emadi, "An improved torque sharing function for torque ripple reduction in switched reluctance machines," *IEEE Trans. Power Electron.*, vol. 34, no. 2, pp. 1635–1644, Feb. 2019.

[2] C. Ho, J. Wang, K. Hu, and C. Liaw, "Development and operation control of a switched-reluctance motor driven flywheel," *IEEE Trans. Power Electron.*, vol. 34, no. 1, pp. 526–537, Jan. 2019.

[3] L. Ge, I. Ralev, A. Klein-Hessling, S. Song, and R. W. De Doncker, "A simple reluctance calibration strategy to obtain the flux-linkage characteristics of switched reluctance machines," *IEEE Trans. Power Electron.*, vol. 35, no. 3, pp. 2787–2798, Mar. 2020.

[4] S. Zossak, M. Stulraiter, P. Makys, and M. Sumega, "Initial position detection of PMSM," in *Proc. IEEE 9th Int. Symp. Sensorless Control Elect. Drives*, 2018, pp. 12–17.

[5] M. U. Jamil, W. Kongprawechnon, and N. Chayopitak, "Eliminating starting hesitation for reliable operation of switched reluctance motor without machine parameters for light electric vehicle applications," *IET Elect. Power Appl.*, vol. 13, no. 7, pp. 996–1003, 2019.

[6] M. Ehsani and B. Fahimi, "Elimination of position sensors in switched reluctance motor drives: State of the art and future trends," *IEEE Trans. Ind. Electron.*, vol. 49, no. 1, pp. 40–47, Feb. 2002.

[7] A. Khalil *et al.*, "Four-quadrant pulse injection and sliding mode observer based sensorless operation of a switched reluctance machine over entire speed range including zero speed," in *Proc. 14th IAS Annu. Meeting Conf. Rec. Ind. Appl. Conf.*, 2005, vol. 3, pp. 2147–2154.

[8] C. Gong, Y. Hu, J. Gao, Y. Wang, and L. Yan, "An improved delay-suppressed sliding-mode observer for sensorless vector-controlled PMSM," *IEEE Trans. Ind. Electron.*, vol. 67, no. 7, pp. 5913–5923, Jul. 2020.

[9] F. Peng, J. Ye, A. Emadi, and Y. Huang, "Position sensorless control of switched reluctance motor drives based on numerical method," *IEEE Trans. Ind. Appl.*, vol. 53, no. 3, pp. 2159–2168, May/Jun. 2017.

[10] C. Lascu and G. Andreescu, "PLL position and speed observer with integrated current observer for sensorless PMSM drives," *IEEE Trans. Ind. Electron.*, vol. 67, no. 7, pp. 5990–5999, Jul. 2020.

[11] I. Ralev, F. Qi, B. Burkhart, A. Klein-Hessling, and R. W. D. Doncker, "Impact of smooth torque control on the efficiency of a high-speed automotive switched reluctance drive," *IEEE Trans. Ind. Appl.*, vol. 53, no. 6, pp. 5509–5517, Nov. 2017.

[12] A. T. Nguyen and D. C. Lee, "Sensorless control of DFIG wind turbine systems based on SOGI and rotor position correction," *IEEE Trans. Power Electron.*, vol. 36, no. 5, pp. 5486–5495, May 2021.

[13] J. Cai, Z. Liu, and Y. Zeng, "Aligned position estimation based fault-tolerant sensorless control strategy for SRM drives," *IEEE Trans. Power Electron.*, vol. 34, no. 8, pp. 7754–7762, Aug. 2019.

[14] D. Xiao, J. Ye, G. Fang, Z. Xia, X. Wang, and A. Emadi, "Improved feature-position-based sensorless control scheme for SRM drives based on nonlinear state observer at medium and high speeds," *IEEE Trans. Power Electron.*, vol. 36, no. 5, pp. 5711–5723, May 2021.

[15] E. Ofori, T. Husain, Y. Sozer, and I. Husain, "A pulse-injection-based sensorless position estimation method for a switched reluctance machine over a wide speed range," *IEEE Trans. Ind. Appl.*, vol. 51, no. 5, pp. 3867–3876, Sep./Oct. 2015.

[16] N. Chen, G. Cao, S. Huang, and J. Sun, "Sensorless control of planar switched reluctance motors based on voltage injection combined with core-loss calculation," *IEEE Trans. Ind. Electron.*, vol. 67, no. 7, pp. 6031–6042, Jul. 2020.

[17] I. Ralev, J. Schulte, and R. W. De Doncker, "Current gradient based rotor position detection of switched reluctance machines at low speed," in *Proc. IEEE Southern Power Electron. Conf.*, 2017, pp. 1–6.

[18] J. Bu and L. Xu, "Eliminating starting hesitation for reliable sensorless control of switched reluctance motors," *IEEE Trans. Ind. Appl.*, vol. 37, no. 1, pp. 59–66, Jan./Feb. 2001.

[19] M. Krishnamurthy, C. S. Edrington, and B. Fahimi, "Prediction of rotor position at standstill and rotating shaft conditions in switched reluctance machines," *IEEE Trans. Power Electron.*, vol. 21, no. 1, pp. 225–233, Jan. 2006.

[20] D. van Treek, P. Matuschek, H. J. Brauer, T. Schoenen, and R. W. De Doncker, "An automatic identification of phase inductance for operation of switched reluctance machines without position sensor," in *Proc. IEEE Int. Elect. Mach. Drives Conf.*, 2009, pp. 1005–1009.

[21] L. Shen, J. Wu, and S. Yang, "Initial position estimation in SRM using bootstrap circuit without predefined inductance parameters," *IEEE Trans. Power Electron.*, vol. 26, no. 9, pp. 2449–2456, Sep. 2011.
[22] S. Song, M. Zhang, and L. Ge, "A new fast method for obtaining flux-linkage characteristics of SRM," *IEEE Trans. Ind. Electron.*, vol. 62, no. 7, pp. 4105–4117, Jul. 2015.
[23] Y. Chang and K. W. E. Cheng, "Sensorless position estimation of switched reluctance motor at startup using quadratic polynomial regression," *IET Elect. Power Appl.*, vol. 7, no. 7, pp. 618–626, 2013.
[24] Y. Chang, K. W. E. Cheng, and S. L. Ho, "Type-V exponential regression for online sensorless position estimation of switched reluctance motor," *IEEE/ASME Trans. Mechatronics*, vol. 20, no. 3, pp. 1351–1359, Jun. 2015.
[25] T. Bamba, A. Komatsuzaki, and I. Miki, "Estimation of rotor position for switched reluctance motor at standstill," in *Proc. Power Convers. Conf.*, 2007, pp. 259–263.
[26] J. Cai and Z. Deng, "Sensorless control of switched reluctance motor based on phase inductance vectors," *IEEE Trans. Power Electron.*, vol. 27, no. 7, pp. 3410–3423, Jul. 2012.
[27] C. Gan, F. Meng, Z. Yu, R. Qu, Z. Liu, and J. Si, "Online calibration of sensorless position estimation for switched reluctance motors with parametric uncertainties," *IEEE Trans. Power Electron.*, vol. 35, no. 11, pp. 12307–12320, Nov. 2020.
[28] B. Parreira, S. Rafael, A. J. Pires, and P. J. C. Branco, "Obtaining the magnetic characteristics of an 8/6 switched reluctance machine: From FEM analysis to the experimental tests," *IEEE Trans. Ind. Electron.*, vol. 52, no. 6, pp. 1635–1643, Dec. 2005.
[29] P. Zhang, P. A. Cassani, and S. S. Williamson, "An accurate inductance profile measurement technique for switched reluctance machines," *IEEE Trans. Ind. Electron.*, vol. 57, no. 9, pp. 2972–2979, Sep. 2010.
[30] J. Cai and Z. Deng, "Initial rotor position estimation and sensorless control of SRM based on coordinate transformation," *IEEE Trans. Instrum. Meas.*, vol. 64, no. 4, pp. 1004–1018, Apr. 2015.
[31] J. Agrawal and M. Aware, "Golden section search (GSS) algorithm for maximum power point tracking in photovoltaic system," in *Proc. IEEE 5th India Int. Conf. Power Electron.*, 2012, pp. 1–6.
[32] J. Lu, Y. Hu, and J. Liu, "Analysis and compensation of sampling errors in TPFS IPMSM drives with single current sensor," *IEEE Trans. Ind. Electron.*, vol. 66, no. 5, pp. 3852–3855, May 2019.
[33] Current Transducer LA 55-P, LEM Company, Version 17, 2018. [Online]. Available: https://www.lem.com/sites/default/files/products_datasheets/la_55-p_e.pdf

Lefei Ge (Member, IEEE) was born in China, in 1992. He received the B.S. degree in measurement and control technology and the M.S. degree in electrical engineering from Northwestern Polytechnical University, Xi'an, China, in 2013 and 2016, respectively, and the Dr.-Ing. degree in electrical engineering from RWTH Aachen University, Aachen, Germany, in 2020.

In September 2016, he became a Research Associate with the Institute of Power Electronics and Electrical Drives, RWTH Aachen University. Since 2020, he has been an Associate Professor with the Department of Electrical Engineering, Northwestern Polytechnical University. His research interests include electrical machines and drives with emphasis on switched reluctance machines.

Huihui Xu (Student Member, IEEE) was born in China, in 1991. She received the B.S. degree from TU Kaiserslautern University, Kaiserslautern, Germany, in 2015, and the M.S. degree in electrical engineering from the RWTH Aachen University, Aachen, Germany, in 2017.

Since 2018, she has been a Research Associate with the Institute of Power Electronics and Electrical Drives, RWTH Aachen University. Her research interests include the thermal modeling of electric machines.

Zhenchao Guo was born in China, in 1995. He received the B.S. and M.S. degrees in electrical engineering from Northwestern Polytechnical University, Xi'an, China, in 2018 and 2021, respectively.

Since 2021, he has been an Engineer with the Institute of Aeronautical Optoelectronics. His research interests include the field of electrical drives, in particular, switched reluctance drives and their control.

Shoujun Song (Senior Member, IEEE) received the B.S. and M.S. degrees from Northwestern Polytechnical University, Xi'an, China, in 2003 and 2006, respectively, and the Dr.-Ing. degree from the Technical University of Berlin, Berlin, Germany, in 2009, all in electrical engineering.

He is currently a Professor with the Department of Electrical Engineering, Northwestern Polytechnical University. His research interests include electrical machines and drives with emphasis on switched reluctance machines and permanent magnet machines.

Rik W. De Doncker (Fellow, IEEE) received the Ph.D. degree in electrical engineering from Katholieke Universiteit Leuven, Leuven, Belgium, in 1986.

In 1987, he joined the University of Wisconsin, Madison, WI, USA, as a Visiting Associate Professor. After a short stay as an Adjunct Researcher with the Interuniversity Microelectronics Centre, Leuven, Belgium, he joined, in 1989, the Corporate Research and Development Center, General Electric Company, Schenectady, NY, USA. In 1994, he joined Silicon Power Corporation, Malvern, PA, USA, a former division of General Electric, Inc., as the Vice President of Technology. In 1996, he became a Professor with RWTH Aachen University, Aachen, Germany, where he currently leads the Institute for Power Electronics and Electrical Drives. Since 2006, he has been the Director of the E.ON Energy Research Center, RWTH Aachen University.

Dr. De Doncker was the President of the IEEE Power Electronics Society (PELS) in 2005 and 2006. He was the Founding Chairman of the German IEEE Industry Applications Society PELS Joint Chapter. He was the recipient of the IEEE IAS Outstanding Achievement Award in 2002, the IEEE PES Nari Hingorani Custom Power Award in 2008, the IEEE William E. Newell Power Electronics Award in 2013, and the IEEE Medal in Power Engineering in 2020.